

An evaluation of the GOES-16 rapid scan for nowcasting in Southeastern Brazil: analysis of a severe hailstorm case

Bruno Z. Ribeiro¹, Luiz A. T. Machado¹, Joao H. Huamán Ch.¹, Thiago S. Biscaro¹

Renato Negri¹, Edmilson Freitas², Kathryn W. Mozer³ and Steven J. Goodman⁴

¹*Centro de Previsão de Tempo e Estudos Climáticos, Instituto Nacional de Pesquisas Espaciais
(CPTEC/INPE), Cachoeira Paulista, São Paulo, Brazil*

²*Instituto de Astronomia, Geofísica e Ciências Atmosféricas, Universidade de São Paulo, São Paulo,
Brazil*

³*NOAA/NESDIS/Office of Satellite and Product Operations, College Park, Maryland*

⁴*GOES-R Program/TGA, Huntsville, Alabama*

*Correspondence to: Bruno Z. Ribeiro, Centro de Previsão de Tempo e Estudos Climáticos /Instituto Nacional de Pesquisas Espaciais (CPTEC/INPE), Rodovia Presidente Dutra, km 39, Cachoeira Paulista - SP, Brasil, 12630-000. E-mail: bruno.ribeiro@inpe.br; URL: <http://www.cptec.inpe.br/>

ABSTRACT: The GOES-16 mesoscale domain sector (MDS) scans with one minute intervals are used in this study to analyze a severe thunderstorm case occurred in southeastern Brazil. The main objective is to evaluate the GOES-16 MDS rapid scans against the operational full-disk scans with lower temporal resolution for nowcasting. Data from a C-band radar, observed sounding and a ground-based lightning network are also used in the analysis. A group of thunderstorms formed in the afternoon of 29 November 2017 in an environment of moderate convective available potential energy (CAPE) and deep-layer shear. The storms presented supercell characteristics and an intense lightning activity. The satellite-derived trends with one-minute interval were skillful in detecting thunderstorm intensification, mainly in the developing stage. The

decrease in cloud-top 10.35- μm brightness temperature was accompanied by cloud-top glaciation, increase of small ice particles at cloud top and increase in storm depth. In the mature stage, there is no evident trend in the satellite-derived parameters that could indicate storm intensification, but the cluster area expands. The one-minute scans presented greater lead times relative to 10 and 15 scans, but also presented numerous false alarms due to oscillations in the satellite-derived parameters. The parameters calculated every 5 minutes presented better skill than 10 and 15 minutes and fewer false alarms than one minute.

Keywords: severe thunderstorm; hail; rapid scan; GOES-16; nowcasting; southeastern Brazil

1. Introduction

Nowcasting using satellites entered a new era with the new generation of the Geostationary Operational Environmental Satellite-R Series (GOES-R). The GOES-R Series provides data with unprecedented spatial, temporal and radiometric resolutions with the Advanced Baseline Imager (ABI), as well as lightning data through the Geostationary Lightning Mapper (GLM), and are especially useful for nowcasting in regions with sparse radar coverage (Schmit et al., 2017). Of particular interest for nowcasting purposes is GOES-R Series ABI mesoscale domain sector (MDS) which provides rapid scanning with a temporal resolution of one minute or 30 seconds over a moveable domain of approximately 1,000 km x 1,000 km that can be executed anywhere in the satellite field of view (Schmit et al., 2017). This study focuses on a severe thunderstorm case in Brazil where a one-minute MDS was utilized.

The benefits of satellite scans with high temporal resolution (<5 min interval)

for monitoring thunderstorms are explored in several studies (e.g., Dworak et al., 2012; Bedka et al., 2012; Mecikalski et al., 2016; Apke et al., 2016; Line et al., 2016). Severe thunderstorms with strong updrafts can evolve more rapidly than the operational 15-minute full-disk scans (Bedka et al., 2012; Cintineo et al., 2013), so that higher scanning temporal resolution can improve nowcasting techniques, forecaster situation awareness, and increase the lead time of severe thunderstorm warnings. As an example, Goodman et al. (1988) studied a severe thunderstorm that evolved from no lightning to maximum lightning activity in 7–8 minutes and caused a microburst four minutes after peak lightning activity. Such rapid storm evolutions are not possible to monitor with scans every 15 minutes (Gatlin and Goodman, 2010).

Given that severe thunderstorms can evolve very rapidly, several techniques based on satellite products were developed to identify convective initiation and thunderstorm intensification (e.g., Mecikalski and Bedka, 2006; Mecikalski et al., 2010a; Mecikalski et al., 2010b). Algorithms based on 15-min resolution are useful for forecasters to identify the thunderstorm characteristics. For example, the updraft intensity can be estimated by the rate of decrease of the cloud-top temperature (e.g., Mecikalski et al., 2016) and the cloud-top glaciation can be evaluated by using the tri-spectral difference (e.g., Ackerman et al., 1990; Strabala et al., 1994). The physical properties of the thunderstorms as estimated by satellites can be used to predict the occurrence of severe weather. Even though these algorithms are useful when using 15-min satellite data, several studies show that higher temporal resolution can provide greater lead time when issuing a warning (e.g., Bedka et al., 2015). The present study aims at comparing satellite-derived parameters with different temporal resolutions to evaluate the different lead times and the advantages of using the MDS scanning over South America.

Several studies have used the GOES data to study convection over South America (e.g., Machado et al., 1998; Vila et al., 2008; Durkee and Mote, 2010). Most of these studies focus on the climatological aspects of mesoscale convective systems (Machado et al., 1998; Durkee and Mote, 2010) and extrapolation techniques to forecast convective systems' motion (Vila et al., 2008). Due to the absence of rapid scans over South America, no study has focused on the advantages of using these data in nowcasting in this continent.

During the testing period of the first GOES-R Series satellite (now the operational GOES-16 or GOES East), a one-minute MDS was made available over the Southeastern Brazil region to support the SOS-CHUVA field campaign intense observation period (IOP), between 27 and 31 November 2017. The SOS-CHUVA campaign was motivated by the CHUVA Project (Machado et al., 2014) to develop applications for nowcasting using dual polarization radars and the geostationary satellites. The simultaneous occurrence of the GOES-16 MDS scan, the ground lightning network, and the SOS-CHUVA campaign generated an unprecedented opportunity to study severe thunderstorms in Brazil.

In this study, the GOES-16 one-minute MDS data is used to analyze two severe hailstorms in southeastern Brazil and evaluate the benefits of rapid scans relative to the conventional operational scans. A tracking algorithm applied to the satellite data is used to monitor the storm clusters (Lagrangian analysis). Different channel combinations, area expansion, and cloud top evolution are tested as nowcasting parameters and compared with radar and ground lightning network data. The nowcasting parameters are computed for 1, 5, 10 and 15 minute intervals to evaluate the gain of information and warning lead time for different time resolutions. The main scientific questions raised in this study are:

What are the main differences between the severe storms that occurred in the region in terms of cloud-top microphysical characteristics as inferred by satellite and lightning activity? Do the satellite-derived parameters in severe subtropical storms behave similarly to midlatitude storms previously studied in other regions of the world? Do the one-minute data provide a significant gain in the nowcasting lead time relative to scans with lower temporal resolution?

This paper is organized as follows: Sec. 2 describes the data and methodology; Sec. 3 shows the results, which are divided in the analysis of the pre-convective environment (Sec. 3.1), convective initiation and storm evolution (Sec. 3.2), the temporal variations of the satellite-derived parameters and their use in nowcasting (Sec. 3.3), an evaluation of satellite parameters with different temporal frequencies (Sec. 3.4), and an analysis of the rapid intensification of one of the studied storms (Sec. 3.5); The conclusions are presented and discussed in Sec. 4.

2. Data and methodology

2.1. The SOS-CHUVA campaign

The SOS-CHUVA campaign IOP was held from 27 and 31 November 2017 in the Southeastern Brazil. During this period, the area of the experiment in Southeastern Brazil was sampled by three radars (an X-band, an S-band and a C-band), disdrometers, radiosondes (twice daily and when convection was occurring within the radars coverage area), surface stations and hailpads. Also, the GOES-16 was performing MDS scans with one-minute interval over the SOS-CHUVA area and nearby (Fig. 1).

2.2 *GOES-16 data and satellite-derived parameters*

The GOES-16 ABI (Schmit et al., 2017) channels employed were the 1.6- μm band with 1 km of spatial resolution and the bands 6.19 μm , 8.5 μm , 10.35 μm , 11.2 μm and 12.3 μm with 2 km of spatial resolution, with all data in the original satellite projection. The satellite images were reprojected to an equidistant cylindrical projection with spatial resolution of 2 km to facilitate the tracking of the convective systems.

A clustering method was applied to the GOES-16 data to identify convective systems and calculate the Lagrangian satellite-derived parameters. The method is based on the ForTraCC (Vila et al., 2008), in which a cluster is defined as an area of at least 40 pixels with 10.35- μm brightness temperature (Tb) lower than 235 K. By using the tracking algorithm, it was possible to compute the cloud cluster size and temporal evolution (Machado and Laurent, 2004), and the cloud top Tb in different channels (Mecikalski et al. 2010a; Mecikalski et al. 2010b). Table 1 shows a summary of each satellite-derived parameter with the respective critical values used for monitoring deep convection. In this study, we will use the minimum or maximum value of the parameter in the cluster to evaluate the temporal trends, since extreme values are generally related to the strongest convective updrafts.

One of the main variables used to estimate the convective cloud depth is the 10.35- μm Tb. Lower Tb relates to deeper cloud tops simply because the temperature decreases with height in the troposphere (Adler and Mack, 1986). The updraft strength can be estimated by the temporal derivative of the 10.35- μm Tb (Adler and Fenn, 1979; Mecikalski and Bedka, 2006). In general, cloud-top cooling rates greater than 4 K in 15

minutes indicate a convective updraft, while cooling rates of 8 K in 15 minutes are associated with a vigorous updraft (Mecikalski and Bedka, 2006).

The particle size was estimated using a reflectance of band 1.6 μm , which associate lower (higher) reflectance values with larger (smaller) particle size (Baum et al., 2000). The reflectance values of this band were obtained by converting the reflectance factor to reflectance using $[1/\cos(\theta)]$, where θ is zenithal angle. In this case, due to the fact that reflectance values become undefined with zenithal angles near 90° , only times before 1950 UTC were considered in this study. The difference between 8.5 μm and 11.2 μm , which is not dependent on the zenithal angle, was used to monitor cloud-top ice crystal sizes. This difference is negative in clear regions due to differences in water vapor absorption, while it is positive in cloud tops containing ice crystals. High positive values are associated with small ice crystals and low positive values with larger ice crystals (Ackerman et al. 1990).

The cloud-top glaciation can be monitored using the tri-spectral difference (Ackerman et al. 1990; Strabala et al. 1994), which is based on the different values of water and ice absorption coefficients in the 8.5–12.3- μm range. The absorption coefficients of ice crystals increase more rapidly in the 8.5–11.2- μm band than in the 11.2–12.3- μm band, and the opposite is valid for the water absorption coefficients. The result is that high values of 8.5–11.2- μm Tb differences are associated with ice crystals and high values of 11.2–12.3- μm Tb differences are associated with water droplets. Therefore, positive values of the tri-spectral difference $[(8.5 - 11.2 \mu\text{m}) - (11.2 - 12.3 \mu\text{m})]$ can be attributed to ice crystals and negative values to water droplets.

The difference between 6.19- and 10.35- μm Tb provides estimates of the cloud depth. In this case, negative values are associated with clear regions or shallow clouds,

since the water vapor absorption causes T_b in the $6.19\text{-}\mu\text{m}$ band to be lower than in the $10.35\text{-}\mu\text{m}$ band. An opposite situation occurs in cases of deep convection when the cloud tops reach the tropopause or lower stratosphere. The water vapor that reaches the stratosphere absorbs radiation from the top of the cloud and emits it at the same temperature of this height, which is warmer than the cloud-top temperature in $10.35\ \mu\text{m}$. Therefore, the $6.19\text{--}10.35\text{-}\mu\text{m}$ difference is positive in deep convection (Fritz and Laszlo, 1993; Ackerman 1996; Schmetz et al. 1997; Mecikalski and Bedka, 2006; Machado et al. 2009).

2.3. *Other datasets*

Data from the C-band radar located in Mateus Leme (19.94°S , 43.43°W , 1270 m altitude; Fig. 1b) were also used. The radar has a beam width of 1 degree and generates a volume scan every 5 minutes. This radar is operated by the *Companhia Energética de Minas Gerais* (CEMIG), the Minas Gerais state authority in electrical energy. Unfortunately, polarimetric variables and radial winds data were very noisy in the studied period, thus only the reflectivity is used in this study. The two storms were tracked using the 0.5° plan position indicator (PPI) horizontal reflectivity factor with the reflectivity threshold of 40 dBZ. The centroid of the reflectivity core is used as a proxy for the storm location, which allowed for tracking the position of the storm every 5 minutes (frequency of radar scans).

The lightning data used in this study derives from the BrasilDAT network, which encompasses more than 70 lightning sensors (Earth Networks). The BrasilDAT detection efficiency is greater than 90% (for both intra-cloud and cloud-to-ground lightning flashes)

over southeastern Brazil (Naccarato and Pinto, 2009). In this study, we will use only the total lightning (sum of cloud-to-ground and cloud-to-cloud lightnings), as this quantity was proved to be the most physically related to storm/updraft intensity and provides greater skill in nowcasting than the use of cloud-to-ground lightning alone (e.g., Schultz et al., 2009; Wu et al., 2018). The GLM sensor was being tested during this period, thus we decided to use only BrasilDAT data.

The pre-convective environment was accessed using the Global Forecast System [GFS, from the National Centers of Environmental Prediction (NCEP)] model analysis. The GFS is a T1534 global model with 64 vertical levels starting a new integration every 6 h. The model output is interpolated to a 0.25° resolution grid, which is used in this study. METAR and sounding data of the Confins Airport (SBCF; 19.62°S , 43.67°W ; Fig. 1) were taken from the University of Wyoming website (<http://weather.uwyo.edu/>).

3. Results

On the afternoon of 29 November 2017, severe storms occurred in east-central Minas Gerais state (Fig. 1) and caused severe winds and large hail (Fig. 2). In the city of Caeté, hail of 5 cm in diameter was responsible for widespread damage to buildings and vehicles (Figs. 2a,b). According to the local Civil Defense, 14 people were injured and more than 300 had to leave their homes. More than 2,050 buildings were damaged, with an equivalent cost of nearly US\$ 220,000. This corresponds to nearly 40% of Caeté's annual gross domestic product (using the 2016 values as reference). The cities of Ribeirão das Neves and Pedro Leopoldo (Fig. 1b), located approximately 100 and 120 km, respectively, to the northwest of Caeté, were affected by other storm nearly two hours

after Caeté. Pedro Leopoldo reported 5-cm hail, whereas severe winds and 2-cm hail occurred in Ribeirão das Neves, producing damage to roofs and trees on both cities.

3.1 Pre-convective environment

Figure 3 shows the GFS analysis fields at 1200 UTC 29 November 2017, which is nearly 4 hours before the first storms formed in the region. A broad cyclonic circulation is observed over the Atlantic Ocean with attendant cyclonic vorticity maximum near the coast of Brazil (Fig. 3a). Minas Gerais state is in the northwestern periphery of the cyclonic circulation, where southwesterly flow predominates. There is no cyclonic vorticity maximum upstream of the region that could result in synoptic-scale forcing for ascent over the area. The 500-hPa temperature trough upstream of the affected cities indicated there was relatively cold air moving over the area in the middle troposphere, increasing the thermodynamic instability with time. Also, the 500-hPa temperatures in the region (nearly -9°C) are 1.5 standard deviations below average for 29 November (based on 32-year Climate Forecast System Reanalysis data). Relatively cold air in the midtroposphere is known to favor thermodynamic instability and hail growth (e.g., Johnson and Sugden, 2014). The strongest 500-hPa winds ($>15\text{ m s}^{-1}$) occur along the Brazilian coast, where the upper-level jet is located (not shown).

The 850-hPa level 1200 UTC fields are shown in Fig. 3b. A surface cold front moved northeastwards over the Atlantic Ocean on 28 November (one day before; not shown) and stalled along the higher terrain in the coast of Brazil (Fig. 1). Lower 850-hPa equivalent potential temperature (θ_e) is found over the Atlantic Ocean in association with southeasterly flow, which causes enhanced 1000–700-hPa moisture flux convergence

(MFC) along the Brazilian coast. MFC is also observed along a ridge oriented in the south-southwest to north-northeast direction in central Minas Gerais (Fig. 1b), where the three affected cities are located and the 850-hPa θ_e is higher. The MFC along this ridge occurs due to the east-southeasterly winds at low-levels and serves as a focus for convective initiation after 1600 UTC. These synoptic fields provide evidence that the storms formed under weak synoptic-scale forcing for ascent.

The 1200 UTC 29 November 2017 sounding at SBCF (Fig. 4) depicts a relatively moist air mass between surface and ~ 600 hPa. A mixed layer is observed in the first kilometer above surface indicating the boundary layer mixing due to radiative heating in the beginning of the day (1200 UTC is 0900 local time). Steep temperature lapse rates and lower relative humidity are observed above the 600-hPa level. Even though the most unstable CAPE is only 200 J kg^{-1} at this time, this temperature/dewpoint temperature profile can attain higher instability during the afternoon in response to low-level radiative heating, which corroborates CAPE values in the $1500\text{--}1700 \text{ J kg}^{-1}$ range over the study region at 1800 UTC as estimated by the GFS analysis and the modified 1200 UTC sounding with 1800 UTC surface observations (not shown; the sounding site is no more than 50 km from the area where the storms occurred). The equilibrium level for surface-based parcels is at nearly 180 hPa, where the temperature is approximately -60°C (213 K). Also, the easterly low-level winds turn to southwesterly midlevel winds and cause 0–6-km wind shear of more than 20 m s^{-1} , which is sufficient for severe storms with rotating updrafts (e.g., Thompson et al., 2003). The mean wind between surface and 6 km above ground level is east-northeast at nearly 11 m s^{-1} .

3.2 *Convective initiation and storm evolution*

The estimated time of hailfall in Caeté (Fig. 1b) is 1740 UTC and in Pedro Leopoldo is 1930 UTC. Ribeirão das Neves was affected at nearly 1900 UTC by the same storm that hit Pedro Leopoldo, but the absence of the GOES-16 data between 1852 and 1900 UTC (possibly due to the tests with GOES-R) precludes the analysis of this moment with the rapid scan. The hail occurrence time was estimated based on reports of local officials, videos in social media and radar imagery, and there is an associated error in the estimate of ± 5 minutes. Therefore, we will use a 10-minute period centered in the most probable time of hailfall to account for this error. This study focuses on the two severe thunderstorms that produced 5-cm hail in Caeté and Pedro Leopoldo, which will be referred as Caeté storm (CTS) and Pedro Leopoldo storm (PLS).

Figure 5 shows the evolution of the $10.35\text{-}\mu\text{m}$ Tb from 1630 to 2015 UTC every 15 minutes. The first time the CTS reached Tb colder than 235 K occurs at 1645 UTC (Fig. 5b), which is followed by an increase in the area colder than 235K in the next 45 minutes (Figs. 5c,d). The coldest Tb of the entire CTS life time (212 K at 1736 UTC; Figure 5e) is attained after the system intensification at 1730 UTC (Fig. 5e), nearly 10 minutes before hailfall. The minimum Tb of CTS is relatively high compared to severe storms documented in the literature (e.g., Bedka et al., 2012; Bedka et al., 2015; Bedka et al., 2018). Also, there is no V- or U-shape signature (e.g., Setvák et al., 2010; Setvák et al., 2013) discernible at the CTS top, but a downstream (east-northeastward) propagation of the anvil. At 1745 UTC (Fig. 5f), CTS minimum Tb is over the city of Caeté. After this time (Figs. 5g–j), CTS weakens and dissipates at nearly 1900 UTC (Fig. 5k). No severe thunderstorm signature is observed in the satellite imagery [V-shape, overshooting top or above-cirrus anvil cloud (Bedka et al., 2018)] besides the cloud-top cooling.

The PLS forms at nearly 1800 UTC (Fig. 5g) 100 km west-southwest of CTS. This storm presents a distinct overshooting top at 1845 and 1900 UTC (Figs. 5j,k), when 2-cm hail and damaging winds were registered in Ribeirão das Neves. A V-shape signature, also indicative of a vigorous updraft, is discernible at 1915 UTC (Fig. 5l), 10 minutes before the 5-cm hail fall at Pedro Leopoldo. Noticeably, the PLS has minimum Tb of 203 K, nearly 9 K lower than CTS, which indicates a deeper updraft in PLS storm minutes before hailfall as compared to CTS. The lower minimum Tb in PLS cluster is possibly associated with the greater thermodynamic instability (CAPE) in the northern part of the study area. Other storms that formed near PLS also had minimum Tb lower than storms that formed in the south of the study region or earlier, such as CTS (not shown). The PLS cluster merges with the other cluster farther south at nearly 1935 UTC.

Imagery every one minute allowed the identification of multiple “pulses” of convective intensification and momentary Tb decrease. A similar behavior was observed in other severe storms. Witt et al. (2018), for example, studied the supercell that generated the El Reno, OK, EF5 tornado on 31 May 2013 and noticed multiple updrafts during a quasi-steady phase of the storm occurred after a period of rapid intensification. The storm was distinguished as a classic supercell after the last of these pulses.

Figure 6 shows CTS and PLS radar-derived trajectories along with total lightning between 1645 and 2100 UTC, and the clusters areas with Tb lower than 235 K at the estimated time of hail reports (1740 and 1920 UTC, respectively). The radar-derived trajectories and lightning paths clearly show slow storm motion during the first 40 minutes of the storms lifetimes (trajectory between two first large dots), followed by a leftward turn and acceleration of storm motion. The 0–6-km mean wind derived from the 1200 UTC sounding is shown in Fig. 6 as evidence that the storms were initially

advected by the mean wind but then changed the direction of motion, moving to the left of the mean wind. This behavior is a well-known and extensively documented signature of supercells, long-lived storms with a rotating updraft, since the perturbation pressure gradient associated with the convective core causes a deflection of the storm motion from the mean wind (Rotunno and Klemp, 1982). Long-lived supercells have been previously observed in Brazil (e.g., Nascimento et al., 2014). The individual trajectories of all cloud clusters observed by satellite (not shown) clearly followed the 0–6-km mean wind to the east-northeast whereas the supercells moved north-northeastward.

The 0.5° PPI reflectivity (Fig. 7) also supports that CTS and PLS were supercells. Hook echoes are observed at 1725 UTC in the CTS (Fig. 7a) and at 1925 UTC in the PLS (Fig. 7b). Hook echoes curved to the north are characteristic of cyclonic supercells (left movers) in the Southern Hemisphere (Nascimento et al., 2014), where the warm/moist storm-relative inflow is from the north. The hook echo signature is distinct in several radar scans in the mature stage of CTS and PLS (not shown). Even though CTS was a supercell there was no satellite signature indicating its severity.

The CTS caused more lightning strikes than the PLS in the first hour after initiation (Fig. 6). Both storms indicate an increase in lightning activity before hailfall, which matches the leftward turn of the radar-derived trajectories. This rapid increase in lightning activity that is observed before severe weather occurs is referred to as a lightning jump (Goodman et al., 1988). This pattern also suggests the lightning activity increased when the mesocyclones intensified, since the deviant motion became more pronounced. CTS dissipates nearly one hour after the hail occurrence, but the PLS intensifies after causing hail. CTS dissipation occurs in nearly the same period of PLS intensification. It is possible that the gust front from the CTS intensifies the PLS updraft as reported by

Goodman and Knupp (1993) and others, or the compensatory subsidence from PLS causes CTS weakening.

An interesting aspect of PLS is the increase in lightning activity after the hail occurrence in Pedro Leopoldo (nearly 1930 UTC; Fig. 6). The lightning activity increases from 10–20 strikes per five minutes to 140–160 strikes per five minutes after 1940 UTC. Also, the storm moves faster and the trajectory deflection to the left of the mean 0–6-km wind increases (Fig. 6). There was no report of severe weather after this time, but this can be attributed to the lower population density north of Pedro Leopoldo. This period of rapid intensification of PLS is explored in Section 3.5 as a special analysis of the mature thunderstorm.

3.3 *Temporal evolution of the satellite-derived parameters*

In this section, the one-minute satellite-derived parameters and the lightning density are analyzed. The objective is to evaluate what parameters show better indications of severe weather in the temporal trends and what is the lead time, i.e., the time between a given parameter trend indicates severe weather is likely and the severe weather is observed at surface.

Figure 8 shows the temporal trends in the satellite-derived parameters. The CTS 10.35- μm Tb (Fig. 8a) varies around the value of 225 K before 1705 UTC, when it drops to a minimum of 216 K. This decrease in Tb is observed in the Tb temporal trend (Fig. 8b) as a minimum cooling rate of -3 K min^{-1} . This moment is when the first deep updraft of CTS occurs (Fig. 5d). It is possible that severe weather occurred minutes after this Tb decrease and associated lightning activity increase, but no reports were found. After this

abrupt decrease, T_b remains steady between 220 and 215 K. Another intense updraft occurs after 1728 UTC and causes a T_b decrease of nearly 12 K in 7 minutes, which is equivalent to an average cooling of 1.71 K min^{-1} or 25.65 K in 15 minutes, more than three times greater than the 8 K in 15 minutes threshold of Mecikalski and Bedka (2006) for a vigorous updraft. The decrease in minimum $10.35\text{-}\mu\text{m}$ T_b after 1728 UTC (Fig. 8a) and the minimum T_b temporal trend occurred at 1730 UTC (Fig. 8b) precedes the most probable time of hailfall by nearly 10 minutes. These trends are accompanied by an increase in lightning activity from 19 lightning flashes between 1725 and 1730 UTC to 46 flashes in the next 5 minutes. This lightning activity increase is known as a lightning jump (e.g., Williams et al., 1999; Gatlin and Goodman, 2010; Schultz et al., 2011), and in this case precedes the severe event nearly 10–15 minutes. This lead time of the lightning jump is in agreement with other studies. The negative trend of T_b (Fig. 8b) is the only parameter that shows a signal before the lightning jump, while the other parameters show a signal in phase with the lightning jump.

The updraft observed after 1728 UTC is responsible for an increase in the tri-spectral difference (Fig. 8c), which changes from negative before 1728 UTC to positive after this time, and attains nearly 4°C between 1730 and 1735 UTC. This behavior occurs in response to the increase in cloud-top ice crystals as the updraft penetrates the upper troposphere (Ackerman et al. 1990). The decrease in sizes of the ice particles at the cloud top is the explanation for the increase in albedo (Fig. 8e) as well, since ice reflects more solar radiation in the $1.6\text{-}\mu\text{m}$ band than cloud droplets. The $8.5\text{--}11.2\text{-}\mu\text{m}$ T_b difference behaves very similarly to the other variables, with an increase in the difference preceding the hail event and in phase with the lightning activity. This increase is associated with an increasing amount of ice crystals in the top of the convective cloud. This parameter is the

best to describe the lightning variability behavior.

The 6.19–10.35- μm difference (Fig. 8d) also increases with the time, but the temporal trend is more continuous and only shows the cloud top height is increasing. The stratosphere was at nearly 120 hPa according to the 1200 UTC sounding (Fig. 4) and the minimum tropopause temperature was -77°C (196 K), while the minimum T_b of CTS was 212 K (-61°C), which indicates this storm didn't penetrate in the stratosphere. The 6.19–10.35- μm difference does not describe the short-time storm variability associated to the updraft intensification. The area and area expansion show the same behavior, i.e., capture the intensification but show no short-term variability.

Figure 9 presents the same parameters of Fig. 8, but for the PLS. A clear lightning jump is observed prior to the first severe event (2-cm hail and wind damage in Ribeirão das Neves) at nearly 1900 UTC. The absence of GOES-16 data between 1852 and 1900 UTC precludes the analysis of the one-minute trends, but the trends in the 1852–1900 UTC period show a decrease in 10.35- μm T_b (Fig. 9a), an increase in the tri-spectral (Fig. 9c) and 8.5–11.2- μm differences (Fig. 9f) and an increase in the 1.6- μm albedo (Fig. 9e), all of them indicating an intensification of the convective updraft.

The period before the second severe event caused by PLS (5-cm hail in Pedro Leopoldo) was remarkably different from the periods before the other severe events in terms of lightning activity. A decrease in lightning density occurs after 1900 UTC, and the lightning density remains stable around 20 flashes per 5 minutes until 1930 UTC. The lightning density then increases rapidly at nearly the same time the severe hail occurred in Pedro Leopoldo. This lightning jump seems to have occurred at the same time of the severe event, not before it as commonly observed, though we have no information if hail occurred before. The lightning density increases to more than 150 flashes per 5 minutes

after the severe event, which is one order of magnitude greater than before. This period of high lightning density of PLS will be analyzed in more detail in Sec. 3.5.

The 10.35- μm Tb decreases between 1916 and 1920 UTC in association with a subtle lightning density increase between 1915 and 1920 UTC. In the same period, the other parameters show a *decrease*, but the expected tendencies would be positive in areas of convective invigoration. On the other hand, the values of the satellite-parameters are high compared to the CTS (Fig. 8) and the period preceding the first severe weather event of PLS. For example, the tri-spectral difference (Fig. 9c) varies between 3°C and 8°C before and during the second severe weather event of PLS in Pedro Leopoldo, while it peaks at 4°C before the CTS event. We hypothesize the PLS enters in the mature stage after the first severe weather event, when the 10.35- μm Tb is lower than 210 K. Both the tri-spectral difference (Fig. 9c) and the 8.5–11.2- μm difference (Fig. 9f) indicate there is glaciation and small ice particles at the cloud top, which is associated with an active updraft. The 6.19–10.35- μm difference (Fig. 9d) denotes a slow increase in cloud depth with time, but no jump before the severe event as observed for CTS.

The evolution of PLS to the mature stage is supported by the 10.35- μm Tb, which is lower than 210 K after 1910 UTC. This value is nearly the temperature of the equilibrium level as indicated by the 1200 UTC sounding, which indicates the PLS updraft probably reached the tropopause. When the updraft reaches the tropopause and encounters the stable air in this layer, the primary growth occurs in the horizontal, and it can be seen as an anvil area expansion (Mecikalski et al., 2016). Fig. 10 evidences that the area increases to almost 2000 km² 20–30 minutes before the first PLS severe weather event, decreases after 1852 UTC, and then increases more rapidly after 1900 UTC. This last rapid increase in the PLS cluster area denotes the horizontal expansion of the anvil as

the updraft reaches the tropopause (Mecikalski et al., 2016). At 1932 UTC, the PLS cluster merges with another cluster and the area expansion is not monitored anymore.

3.4 *Comparison of satellite parameters in different temporal resolutions*

In this section, the satellite-derived parameters are plotted for different time resolutions to evaluate the one-minute data against 5-, 10- and 15-minute data. The objective is to verify the potential gain in lead time for hypothetical warnings based on these trigger signals when using the rapid scan.

Figure 11 shows the satellite derived parameters with different temporal resolutions for the CTS cluster. As expected, the one-minute trends show much more variability and details than the other temporal resolutions. The 10.35- μm Tb decrease from 1728 to 1736 UTC (Fig. 11a), which precedes the hail event, is not captured by the 10- and 15-minute resolutions. The minimum 10.35- μm Tb of the entire CTS lifetime (212 K at 1736 UTC) is missed in the 10 and 15-minute resolutions as well. The 5-minute resolution data, however, is able to represent both the Tb drop and the Tb minimum with good similarity to the one-minute data. The lead time of the 10.35- μm Tb is similar to using data with 1 and 5 minutes, but is much lower using data with 10 or 15 minutes. The decrease in Tb and the association of it with the intensification of the CTS updraft would be noted only at the time of the event for the 10- and 15-minute resolutions, and the updraft intensity estimated by Tb trends would be lower (Mecikalski et al., 2016).

The other satellite-derived parameters preceding the CTS hail event (Figs. 11b,c,d) show a similar pattern. The 5-minute curves follow the one-minute curves closely, even though they are not able to capture the one-minute pulses. For the 1.6- μm

albedo (Fig. 11b) the maximum that precedes the CTS event occurs at 1732 UTC (close to 1730 UTC, when both 5-, 10- and 15-minute resolutions have a measurement), and the trends are also observed in the 5-, 10- and 15-minute data. However, the increase in albedo would be noticed at these resolutions only at the time of peak (1730 UTC), while the increase in albedo with one-minute data would be noticed 3 minutes before. The 8.5–11.2- μm differences and the tri-spectral difference present two maxima at nearly 1713 and 1734 UTC and a minimum between them at 1725 UTC. These variations are again better described by the 1- and 5-minute data, which allows a better monitoring of the increases and decreases in storm intensity. The 15-minute curve for the 8.5–11.2- μm difference (Fig. 11c), for example, is not able to depict the minimum at nearly 1725 UTC, and consequently the positive tendency after this time. The 6.19–10.35- μm difference, area and area expansion were not shown because the one-minute image and 15 minutes images are similar and, at least for these events, these parameters do not introduce new information at higher temporal resolutions.

The same graphics are shown for the PLS in Figure 12. Unfortunately for this case, the lack of data between 1852 and 1900 UTC precludes the comparison of 1- and 5-minute resolutions with the other ones. However, the data in other times leads to similar conclusions in comparison to the CTS case: the 5-minute data is able to follow the one-minute data in most of the peaks. Even though the 10- and 15-minute data present a 10.35- μm Tb decrease with time (Fig. 12a), there is no discernible rapid decrease that could be associated with an updraft intensification before the first severe event from PLS, precluding the issuance of a warning. After 1910 UTC, when the PLS enters the mature stage, the trends are less useful in predicting the severe weather occurrences, and the advantages of the 1- and 5-minute data are less evident.

The comparison of the MDS one-minute data with the more conventional scanning resolutions of 5, 10 and 15 minutes evidences the one-minute data shows details that the other resolutions are not able to capture. Variations in cloud-top properties and updraft intensity occurring in a few minutes are only measured by the rapid scan. However, for nowcasting purposes, the 5-minute scans can describe the main tendencies of the satellite-derived parameters and also filter the one-minute trends that may not be associated directly with a trend in storm intensity. A warning system based on the one-minute data without any temporal filter could cause too many false alarms. An example appears in the trends of the tri-spectral difference for the PLS (Fig. 12d) between 1905 and 1940 UTC, in which the one-minute data shows several maxima and minima within an oscillatory pattern while the 5-minute data presents a smoothed curve indicating a more stable tendency of the parameter. The one-minute trends in this case could lead to false alarms. A possible explanation for the good results using 5-minute data is the fact that most updrafts accompanied by Tb decrease occur in the range between 5 and 10 minutes, which allows at least one measurement if the Tb drop with 5-minutes interval. The indication of severe weather by the 10- and 15-minutes trends is better before the first PLS event (Fig. 12) than before the CTS event (Fig. 11), which indicates that there is a case-to-case variability in the skill of each scan frequency. This analysis relies on only two cases and a statistical analysis with a high number of cases is deserved.

3.5 *Period of rapid intensification of PLS*

In this section, the period of rapid intensification of the PLS after 1940 UTC is analyzed. No severe weather reports were found in this period, but the lightning trends

suggest that the PLS intensified even further after the 5-cm hailfall in Pedro Leopoldo at nearly 1930 UTC. Figure 7 shows the increase in lightning density after the storm passes Pedro Leopoldo County and also the wider area where lightning is observed, suggesting an area expansion of the storm. This area expansion is confirmed in the trend shown in Fig. 10 before the merger of PLS with the other cluster farther south.

The satellite-derived parameters and lightning density in this period are shown in Fig. 13. The lightning density increase is evident after 1930 UTC, when the lightning density increases from nearly 30 to more than 150 lightning flashes per 5 minutes in a period of roughly 30 minutes. The radar reflectivity signature (not shown) shows a prominent hook echo at this time, which is a signature of updraft rotation and presence of a mesocyclone in the thunderstorm. It is possible that the mesocyclone played a role on the maintenance of the PLS by inducing greater thunderstorm organization and limiting the disruption of the updraft by the downdraft (e.g., Houze, 2004).

The $10.35\text{-}\mu\text{m}$ Tb (Fig. 13a) varies between 209 and 202 K in the period, which is slightly lower than the estimated temperature of the equilibrium layer (210 K). Some updrafts are more intense and cause momentary $10.35\text{-}\mu\text{m}$ Tb decrease, such as between 1940 and 1945 UTC and 2012 and 2017 UTC, but there is no total trend in $10.35\text{-}\mu\text{m}$ Tb in the period. The tri-spectral difference (Fig. 13c) and $8.5\text{--}11.2\text{-}\mu\text{m}$ Tb difference (Fig. 13b) indicates glaciation at the cloud top, which is evident given the temperatures well below -38°C (Mecikalski et al., 2016). The difference between $6.9\text{-}\mu\text{m}$ Tb and $10.35\text{-}\mu\text{m}$ Tb (Fig. 13d) is steady at nearly -2°C , which indicates the thunderstorm depth remains constant during the period and reinforces the idea that the updrafts are not able to reach the stratosphere (overshoot) in this case. As the storm expands and attains the mature stage, the variability of the parameters decreases, and the one-minute scans do not

produce additional information of the storm for nowcasting purposes.

4. Conclusions

Two storms responsible for severe hail and wind reports in southeastern Brazil were analyzed using the GOES-16 MDS scans. Lagrangian satellite-derived quantities commonly used in nowcasting were calculated for these storms by using a cluster tracking algorithm. The analysis benefited from data of a C-band radar and a lightning detection network in the same region.

The pre-convective environment was characterized by a midlevel trough moving northeastward over the Atlantic Ocean, with relatively cold air ($-9\text{ }^{\circ}\text{C}$ in 500 hPa) and high wind speeds (30–40 kt) over southeastern Brazil. The 10–20-kt easterly low-level flow, in association with the strong midlevel flow and moderate thermodynamic instability (estimated surface-based CAPE between 1500 and 1700 J kg^{-1} during late afternoon), even though not exceptional, favored severe, rotating thunderstorms in the area. Most storms in the afternoon were triggered along a north-south orographic ridge where the moisture flux convergence was enhanced by the low-level easterly winds.

The severe storm responsible for 5-cm hail in Caeté (CTS) presented a clear deviant motion to the left of the mean wind and a hook echo signature on radar, a characteristic of supercell storms. This storm was interesting because it did not present characteristics of a severe thunderstorm in satellite imagery. The minimum cloud-top $10.35\text{-}\mu\text{m}$ T_b was 212 K, which is higher than the minimum of other storms nearby. The satellite-derived parameters indicate the CTS probably did not reach the equilibrium level at the tropopause, which relates to its relatively warm cloud top. Between 10 and 15

minutes before the occurrence of hail caused by the CTS, the satellite-derived parameters showed a rapid decrease in 10.35- μm Tb (peaking at -3 K per minute), which is much more intense than the decrease rates found by Mecikalski and Bedka (2006) using satellite data with 15 minutes of temporal resolution. A lightning jump was also observed during this period. The other parameters also indicated an updraft invigoration prior to the severe weather event: an increase in 1.6- μm albedo suggesting increasing small ice particles at the cloud top and an increase in both the trispectral and the 8.5–11.2- μm differences indicating cloud-top glaciation. The 6.19–10.35- μm difference shows an increase in value, but does not show any signature of penetrative cloud and does not show the short-time variability, but a nearly continuous monotonic increase in the cloud depth. The 6.19–10.35- μm difference did not attain positive values, which corroborates that an overshooting top was not observed in the CTS. The CTS weakens after the severe weather event and dissipates at nearly 1900 UTC.

The PLS presented supercell characteristics and produced two severe weather events at different times. For the first event, which occurred nearly one hour after initiation, the satellite-derived parameters behaved similarly to the CTS and suggested convective invigoration, even though there was no one-minute GOES-16 data just before the first PLS severe weather event. The parameters indicate a rapid decrease in cloud-top temperature, increase in cloud-top glaciation and increase in storm depth 10-15 minutes before the event, plus a lightning jump.

The second event occurred during the transition to the mature stage, when the satellite-derived parameters stabilize and subsequently the lightning density increases. Therefore, there are no clear tendencies in the satellite-derived parameters that could indicate updraft invigoration, but only the maintenance of an intense updraft. It is also

possible that severe weather occurred between the first and the second PLS events, but no reports were found.

The PLS evolved to the mature stage after 1940 UTC, with lightning densities over 150 lightning flashes per 5 minutes in some moments and a relative stability of the satellite derived parameters, along with 10.35- μm near and below the equilibrium level temperature. It is possible that the deeper updraft and greater cloud-top glaciation of the PLS are associated with a sustained mesocyclone that maintained the storm organization for more time than the CTS. The area where the PLS formed and the time of the day (late afternoon) suggest the CAPE was higher than when the CTS formed, which could have contributed to a deeper storm.

Other interesting conclusions for this event are: a) the minimum cloud-top 10.35- μm Tb and the Tb cooling rate have a lead time to the lightning activity, while the other parameters are in phase with the lightning activity, even though all parameters have a lead time to the hail occurrence; b) the satellite-derived parameters for these storms present high time variability in the range of 1 to 5 minutes in the initiation and maturation stages, but as the storm becomes mature (such as PLS after 1940 UTC), this variability is reduced.

The advantages of the rapid scan in nowcasting are clear when comparing the one-minute data with the operational 15-minute data. There are several rapid oscillations in the storm intensity, such as updraft intensity, glaciation and depth changes, that are only perceivable using the one-minute data. This is in agreement with Mecikalski et al. (2016), which showed the one-minute 10.35- μm Tb has good correlation with the amount of CAPE in the layer where the updraft is occurring. On the other hand, the 5-minute data showed good representation of the storm-scale oscillations in the cases studied. Also, the

5-minute data is able to smooth the oscillations shown in the one-minute data and can facilitate the nowcasting process by reducing the false alarm. A meteorologist monitoring the one-minute parameters trend would see several positive and negative trends that do not precede severe weather.

This paper uses data from a GOES-16 MDS one-minute scan over southeastern Brazil and a C-band radar to analyze two severe storms that produced large hail and wind damage. The one-minute trends in the satellite-derived parameters proved to be an important tool for nowcasting and much better at describing storm intensity fluctuations than the operational 15-minute scans mainly for the convective initiation and maturation periods. The study suggests the investigation of other cases to understand this change of time variability as the storm evolve during the life cycle. The ability of 5-minute scans to describe the most important trends in storm intensity can be used to plan operational procedures in satellite scans in the future. Scans of the entire GOES area at 5 minute intervals, for example, can help improve nowcasting over a large area, while the rapid scans only focus on a small domain.

Acknowledgements

The authors acknowledge NOAA NESDIS for providing the MDS scan over the SOS CHUVA area, the CEMIG for providing the Mateus Leme C-band radar data, the Civil Defense of Minas Gerais (Diretoria de Controle de Emergências) for damage information, the Group of Atmospheric Electricity (ELAT) from INPE for the BrasilDAT lightning data. The scientific results and conclusions, as well as any views or opinions expressed herein, are those of the author(s) and do not necessarily reflect those of NOAA or the Department of Commerce. This study was supported by FAPESP (grant

2015/14497-0).

References

Adler, R. F., & Fenn, D. D. (1979). Thunderstorm vertical velocities estimated from satellite data. *Journal of the Atmospheric Sciences*, 36(9), 1747-1754.

Adler, R. F., & Mack, R. A. (1986). Thunderstorm cloud top dynamics as inferred from satellite observations and a cloud top parcel model. *Journal of the atmospheric sciences*, 43(18), 1945-1960.

Ackerman, S. A., Smith, W. L., Revercomb, H. E., & Spinhirne, J. D. (1990). The 27–28 October 1986 FIRE IFO Cirrus Case Study: Spectral Properties of Cirrus Clouds in the 8–12 μm Window. *Monthly Weather Review*. [https://doi.org/10.1175/1520-0493\(1990\)118<2377:TOFICC>2.0.CO;2](https://doi.org/10.1175/1520-0493(1990)118<2377:TOFICC>2.0.CO;2).

Ackerman, S. A. (1996). Global satellite observations of negative brightness temperature differences between 11 and 6.7 μm . *Journal of the atmospheric sciences*, 53(19), 2803-2812.

Apke, J. M., Mecikalski, J. R., & Jewett, C. P. (2016). Analysis of mesoscale atmospheric flows above mature deep convection using super rapid scan geostationary satellite data. *Journal of Applied Meteorology and Climatology*, 55(9), 1859-1887.

Baum, B. A., Soulen, P. F., Strabala, K. I., King, M. D., Ackerman, S. A., Menzel, W. P., & Yang, P. (2000). Remote sensing of cloud properties using MODIS airborne simulator imagery during SUCCESS: 2. Cloud thermodynamic phase. *Journal of Geophysical Research: Atmospheres*, 105(D9), 11781–11792. <https://doi.org/10.1029/1999JD901090>.

Bedka, K. M., Dworak, R., Brunner, J., & Feltz, W. (2012). Validation of satellite-based objective overshooting cloud-top detection methods using CloudSat cloud profiling radar observations. *Journal of Applied Meteorology and Climatology*, *51*(10), 1811-1822.

Bedka, K. M., Wang, C., Rogers, R., Carey, L. D., Feltz, W., & Kanak, J. (2015). Examining deep convective cloud evolution using total lightning, WSR-88D, and GOES-14 super rapid scan datasets. *Weather and Forecasting*, *30*(3), 571-590.

Bedka, K., Murillo, E. M., Homeyer, C. R., Scarino, B., & Mersiowsky, H. (2018). The Above-Anvil Cirrus Plume: An Important Severe Weather Indicator in Visible and Infrared Satellite Imagery. *Weather and Forecasting*, *33*(5), 1159-1181.

Cintineo, J. L., Pavolonis, M. J., Sieglaff, J. M., & Heidinger, A. K. (2013). Evolution of severe and nonsevere convection inferred from GOES-derived cloud properties. *Journal of Applied Meteorology and Climatology*, *52*(9), 2009-2023.

Durkee, J. D., & Mote, T. L. (2010). A climatology of warm-season mesoscale convective complexes in subtropical South America. *International Journal of Climatology*, *30*(3), 418-431.

Dworak, R., Bedka, K., Brunner, J., & Feltz, W. (2012). Comparison between GOES-12 overshooting-top detections, WSR-88D radar reflectivity, and severe storm reports. *Weather and Forecasting*, *27*(3), 684-699.

Fritz, S., & Laszlo, I. (1993). Detection of water vapor in the stratosphere over very high clouds in the tropics. *Journal of Geophysical Research: Atmospheres*, *98*(D12), 22959-22967.

Gatlin, P. N., & Goodman, S. J. (2010). A total lightning trending algorithm to identify severe thunderstorms. *Journal of atmospheric and oceanic technology*, *27*(1), 3-

22.

Goodman, S. J., Buechler, D. E., Wright, P. D., & Rust, W. D. (1988). Lightning and precipitation history of a microburst-producing storm. *Geophysical research letters*, 15(11), 1185-1188.

Goodman, S. J., and K.R. Knupp. Tornadogenesis via squall line and supercell interaction: The November 15, 1989 Huntsville, Alabama tornado, *The Tornado: Its Structure, Dynamics, Prediction, and Hazards*, AGU Geophys. Monogr. Series, 79, 183-199, 1993.

Houze, R. A. (2004). Mesoscale convective systems. *Reviews of Geophysics*, 42(4).

Johnson, A. W. and K. E. Sugden, 2014: Evaluation of sounding-derived thermodynamic and wind-related parameters associated with large hail events. *Electronic J. Severe Storms Meteor.*, 9 (5), 1–42.

Line, W. E., Schmit, T. J., Lindsey, D. T., & Goodman, S. J. (2016). Use of geostationary super rapid scan satellite imagery by the Storm Prediction Center. *Weather and Forecasting*, 31(2), 483-494.

Machado, L. A. T., Rossow, W. B., Guedes, R. L., & Walker, A. W. (1998). Life cycle variations of mesoscale convective systems over the Americas. *Monthly Weather Review*, 126(6), 1630-1654.

Machado, L. A. T., & Laurent, H. (2004). The convective system area expansion over Amazonia and its relationships with convective system life duration and high-level wind divergence. *Monthly weather review*, 132(3), 714-725.

Machado, L. A., Lima, W. F., Pinto Jr, O., & Morales, C. A. (2009). Relationship between cloud-to-ground discharge and penetrative clouds: A multi-channel satellite

application. *Atmospheric Research*, 93(1-3), 304-309.

Machado, L. A., Silva Dias, M. A., Morales, C., Fisch, G., Vila, D., Albrecht, R., ... & Cohen, J. (2014). The CHUVA project: How does convection vary across Brazil?. *Bulletin of the American Meteorological Society*, 95(9), 1365-1380.

Mecikalski, J. R., & Bedka, K. M. (2006). Forecasting convective initiation by monitoring the evolution of moving cumulus in daytime GOES imagery. *Monthly Weather Review*, 134(1), 49-78.

Mecikalski, J. R., MacKenzie Jr, W. M., Koenig, M., & Muller, S. (2010a). Cloud-top properties of growing cumulus prior to convective initiation as measured by Meteosat Second Generation. Part I: Infrared fields. *Journal of Applied Meteorology and Climatology*, 49(3), 521-534.

Mecikalski, J. R., MacKenzie Jr, W. M., König, M., & Muller, S. (2010b). Cloud-top properties of growing cumulus prior to convective initiation as measured by Meteosat Second Generation. Part II: Use of visible reflectance. *Journal of Applied Meteorology and Climatology*, 49(12), 2544-2558.

Mecikalski, J. R., Jewett, C. P., Apke, J. M., & Carey, L. D. (2016). Analysis of cumulus cloud updrafts as observed with 1-min resolution Super Rapid Scan GOES imagery. *Monthly Weather Review*, 144(2), 811-830.

Naccarato, K. P., & Pinto Jr, O. (2009). Improvements in the detection efficiency model for the Brazilian lightning detection network (BrasilDAT). *Atmospheric Research*, 91(2-4), 546-563.

Nascimento, E. L., Held, G., & Gomes, A. M. (2014). A Multiple-Vortex Tornado in Southeastern Brazil. *Monthly Weather Review*, 142(9), 3017-3037.

Rotunno, R., & Klemp, J. B. (1982). The influence of the shear-induced pressure

gradient on thunderstorm motion. *Monthly Weather Review*, 110(2), 136-151.

Schmetz, J., Tjemkes, S. A., Gube, M., & Van de Berg, L. (1997). Monitoring deep convection and convective overshooting with METEOSAT. *Advances in Space Research*, 19(3), 433-441.

Schmit, T. J., Goodman, S. J., Gunshor, M. M., Sieglaff, J., Heidinger, A. K., Bachmeier, A. S., ... & Rudlosky, S. (2015). Rapid Refresh information of significant events: Preparing users for the next generation of geostationary operational satellites. *Bulletin of the American Meteorological Society*, 96(4), 561-576.

Schmit, T. J., Griffith, P., Gunshor, M. M., Daniels, J. M., Goodman, S. J., & Lebar, W. J. (2017). A closer look at the ABI on the GOES-R series. *Bulletin of the American Meteorological Society*, 98(4), 681-698.

Schultz, C. J., Petersen, W. A., & Carey, L. D. (2009). Preliminary development and evaluation of lightning jump algorithms for the real-time detection of severe weather. *Journal of Applied Meteorology and Climatology*, 48(12), 2543-2563.

_____, _____, & _____, 2011: Lightning and severe weather: A comparison between total and cloud-to-ground lightning trends. *Wea. Forecasting*, 26, 744-755, doi:10.1175/WAF-D-10-05026.1.

Setvák, M., Lindsey, D. T., Novák, P., Wang, P. K., Radová, M., Kerkmann, J., ... & Charvát, Z. (2010). Satellite-observed cold-ring-shaped features atop deep convective clouds. *Atmospheric Research*, 97(1-2), 80-96.

Setvák, M., Bedka, K., Lindsey, D. T., Sokol, A., Charvát, Z., Štáskta, J., & Wang, P. K. (2013). A-Train observations of deep convective storm tops. *Atmospheric research*, 123, 229-248.

Strabala, K. I., Ackerman, S. A., & Menzel, W. P. (1994). Cloud properties inferred from 8–12- μ m data. *Journal of Applied Meteorology*, 33(2), 212-229.

Thompson, R. L., Edwards, R., Hart, J. A., Elmore, K. L., & Markowski, P. (2003). Close proximity soundings within supercell environments obtained from the Rapid Update Cycle. *Weather and Forecasting*, 18(6), 1243-1261.

Vila, D. A., Machado, L. A. T., Laurent, H., & Velasco, I. (2008). Forecast and Tracking the Evolution of Cloud Clusters (ForTraCC) using satellite infrared imagery: Methodology and validation. *Weather and Forecasting*, 23(2), 233-245.

Williams, E.R., B. Boldi, A. Matlin, M. Weber, S. Hodanish, D. Sharp, S. Goodman, R. Raghavan, and D. Buechler, The Behavior of Total Lightning Activity in Severe Florida Thunderstorms, Special Issue of Atmospheric Research, 51, 245-265, 1999.

Witt, A., Burgess, D. W., Seimon, A., Allen, J. T., Snyder, J. C., & Bluestein, H. B. (2018). Rapid-scan Radar Observations of an Oklahoma Tornadic Hailstorm producing Giant Hail. *Weather and Forecasting*, (2018).

Wu, F., Cui, X., & Zhang, D. L. (2018). A lightning-based nowcast-warning approach for short-duration rainfall events: Development and testing over Beijing during the warm seasons of 2006–2007. *Atmospheric Research*, 205, 2-17.

Table 1: Interest fields and critical values.

Physical attribute	Interest field	Critical values
Particle size	1.6- μm reflectivity	Low values \rightarrow large particles size High values \rightarrow small particles size
	8.5- μm Tb – 11.2- μm Tb	High positive values \rightarrow large ice crystals Low negative values \rightarrow large ice crystals
Cloud-top glaciation	(8.5- μm Tb – 11.2- μm Tb) – (11.2- μm Tb – 12.3- μm Tb)	$> 0 \rightarrow$ ice crystals $< 0 \rightarrow$ water droplets
Cloud depth	6.19- μm Tb – 10.35- μm Tb	> -10 K \rightarrow deep cloud
	10.35- μm Tb	Tb < 273 K \rightarrow deep cloud
Updraft strength	Temporal derivative of 10.35- μm Tb	dTb < -4 K/15 min \rightarrow vigorous updraft

List of figure captions:

FIGURE 1: Map showing the study region in the Minas Gerais state, southeastern Brazil, and the areas of the affected counties (Caeté, Ribeirão das Neves and Pedro Leopoldo). The GOES-16 rapid scan area during 29 November 2017 is delimited by the blue polygon. The red dot is the location of Mateus Leme C-band radar (19.94°S, 43.43°W, 1270 m altitude) and the red circle is the area covered by the radar (250-km radius). The magenta star is the location of the SBCF sounding site. The state of Minas Gerais in southeastern Brazil is also indicated.

FIGURE 2: Photos of the hailstones and associated damage on 29 November 2017. (a) 4–5-cm hailstones from the CTS and (b) hail accumulation in a street of Pedro Leopoldo.

FIGURE 3: GFS analysis at 1200 UTC 29 November 2017. (a) 500-hPa relative vorticity (10^{-5} s^{-1} , shaded), temperature ($^{\circ}\text{C}$, grey dashed contours), geopotential height (dam, thick black contours every 6 dam) and winds (m s^{-1} , pennant is 25 m s^{-1} , full barb is 5 m s^{-1} , and half barb is 2.5 m s^{-1}). (b) 850-hPa θ_e (K, shaded), geopotential height (dam, thick black contours every 1 dam) and winds (m s^{-1} , pennant is 25 m s^{-1} , full barb is 5 m s^{-1} , and half barb is 2.5 m s^{-1}), and 1000–700-hPa MFC ($10^{-5} \text{ g kg}^{-1} \text{ s}^{-1}$, thin grey contours every $3 \times 10^{-5} \text{ g kg}^{-1} \text{ s}^{-1}$ starting at $3 \times 10^{-5} \text{ g kg}^{-1} \text{ s}^{-1}$). Contours of the cities affected by severe weather are drawn.

FIGURE 4: Skew T/log p diagram showing the 1200 UTC sounding at Confins Airport (19.62°S, 43.67°W; Fig. 1) where the continuous line indicates the temperature and the dashed line the dewpoint temperature. The severe weather parameters calculated with the sounding data are surface-based CAPE (SBCAPE), most unstable CAPE (MUCAPE), downdraft CAPE (DCAPE), 0–1-km and 0–3-km storm-relative helicity

(SRH), and 0–6-km and 0–1-km wind shear magnitude.

FIGURE 5: GOES-16 10.35- μm Tb (K) at (a) 1630, (b) 1645, (c) 1700, (d) 1715, (e) 1730, (f) 1745, (g) 1800, (h) 1815, (i) 1830, (j) 1845, (k) 1900, (l) 1915, (m) 1930, (n) 1945, (o) 2000 and (p) 2015 UTC. The CTS cluster, PLS cluster, and other noteworthy features are indicated in the figures, as well as the occurrences of hail in each estimated time. All images were displaced to account for the parallax error.

FIGURE 6: GOES-16 10.35- μm Tb (K, shaded) in the CTS and PLS clusters ($\text{Tb} < 235$ K) at 1740 and 1920 UTC (5–10 minutes before hail reports), respectively, BrasilDAT total flashes (magenta dots, accumulated in 5-minute intervals according to the colorbar) and CTS and PLS trajectories derived from the 0.5° plan position indicator reflectivity centroids at each 5 minutes. The Caeté, Ribeirão das Neves and Pedro Leopoldo counties areas are delimited by thin black contours. The small squares along the storms trajectories indicate the time every 5 minutes, and the larger squares the time every 40 minutes (UTC, numbers at the left of the squares). The satellite-derived clusters were displaced to account for the parallax error.

FIGURE 7: Mateus Leme C-band radar 0.5° plan position indicator reflectivity factor (dBZ) at (a) 1745 UTC and (b) 1925 UTC, the approximate times of occurrence of hail in Caeté and Pedro Leopoldo, respectively.

FIGURE 8: Temporal variation of (a) minimum 10.35- μm Tb (K, red line), (b) temporal trend of 10.35- μm Tb (K min^{-1} , black line), (c) maximum tri-spectral difference (K, green line), (d) maximum difference between 6.19- μm Tb and 10.35- μm Tb (K, magenta line), (e) maximum 1.6- μm albedo (yellow line) and (f) maximum difference between 8.5- μm Tb and 11.2- μm Tb (K, dark red line) for the CTS cluster using GOES-16 data every one minute. The blue dashed line is the lightning strikes density (right

vertical axis). The lightning density value is centered in the middle of the 5-minute period of accumulation. The shaded area is the estimated time of hailfall in Caeté. In the X axis, the colored labels are minutes relative to hailfall and black labels are time (UTC). The main physical processes associated with the trends are described.

FIGURE 9: Same as Figure 8, but for the PLS cluster. The leftmost shaded area is the Ribeirão das Neves 2-cm hail and wind event and the rightmost shaded area is the Pedro Leopoldo 5-cm hail event. In the X axis, the colored labels are minutes relative to hailfall (for each event according to the color) and black labels are time (UTC). The main physical processes associated with the trends are described.

FIGURE 10: Temporal variation of the PLS cluster area (km²). The leftmost shaded area is the Ribeirão das Neves 2-cm hail and wind event and the rightmost shaded area is the Pedro Leopoldo 5-cm hail event. In the X axis, the colored labels are minutes relative to hailfall (for each event according to the color) and black labels are time (UTC).

FIGURE 11: Temporal variations of the satellite-derived parameters each 1 (blue dotted line), 5 (magenta dot-dashed line), 10 (orange dashed line) and 15 (green continuous line) minutes for the CTS cluster. (a) Minimum 10.35- μm Tb (K), (b) maximum 1.6- μm albedo, (c) maximum difference between 8.5- μm Tb and 11.2- μm Tb (K) and (d) maximum tri-spectral difference (K). The shaded area is the estimated time of hailfall in Caeté. In the X axis, the colored labels are minutes relative to hailfall and black labels are time (UTC).

FIGURE 12: Temporal variations of the satellite-derived parameters each 1 (blue dotted line), 5 (magenta dot-dashed line), 10 (orange dashed line) and 15 (green continuous line) minute for the PLS cluster. (a) Minimum 10.35- μm Tb (K), (b) maximum difference between 6.9- μm Tb and 10.35- μm Tb (K), (c) maximum difference between

8.5- μm Tb and 11.2- μm Tb (K) and (d) maximum tri-spectral difference (K). The leftmost shaded area is the Ribeirão das Neves 2-cm hail and wind event and the rightmost shaded area is the Pedro Leopoldo 5-cm hail event. In the X axis, the colored labels are minutes relative to hailfall (for each event according to the color) and black labels are time (UTC).

FIGURE 13: Temporal variation of (a) minimum 10.35- μm Tb (K, red line), (b) maximum difference between 8.5- μm Tb and 11.2- μm Tb (K, dark red line), (c) maximum tri-spectral difference (K, green line) and (d) maximum difference between 6.19- μm Tb and 10.35- μm Tb (K, magenta line) for the PLS cluster mature stage using GOES-16 data every one minute. The blue dashed line is the lightning strikes density (right vertical axis). The lightning density value is centered in the middle of the 5-minute period of accumulation. The shaded area is the estimated time of hailfall in Pedro Leopoldo.

List of figures:

FIGURE 1:

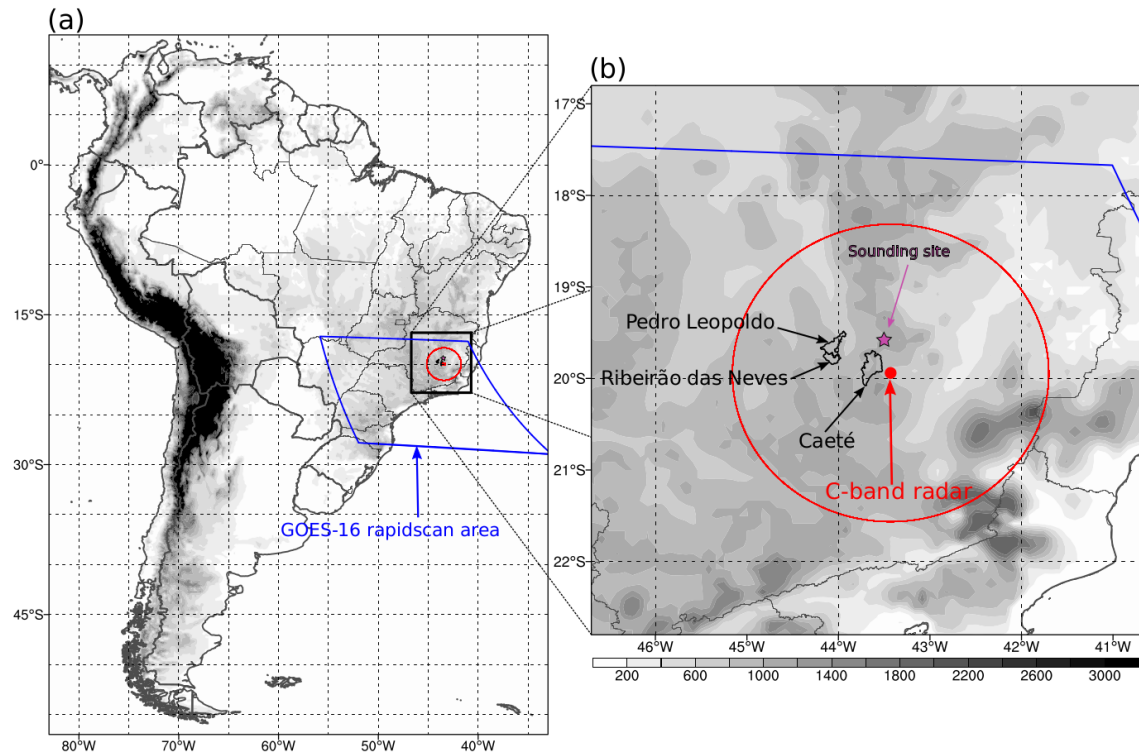


FIGURE 2:



FIGURE 3:

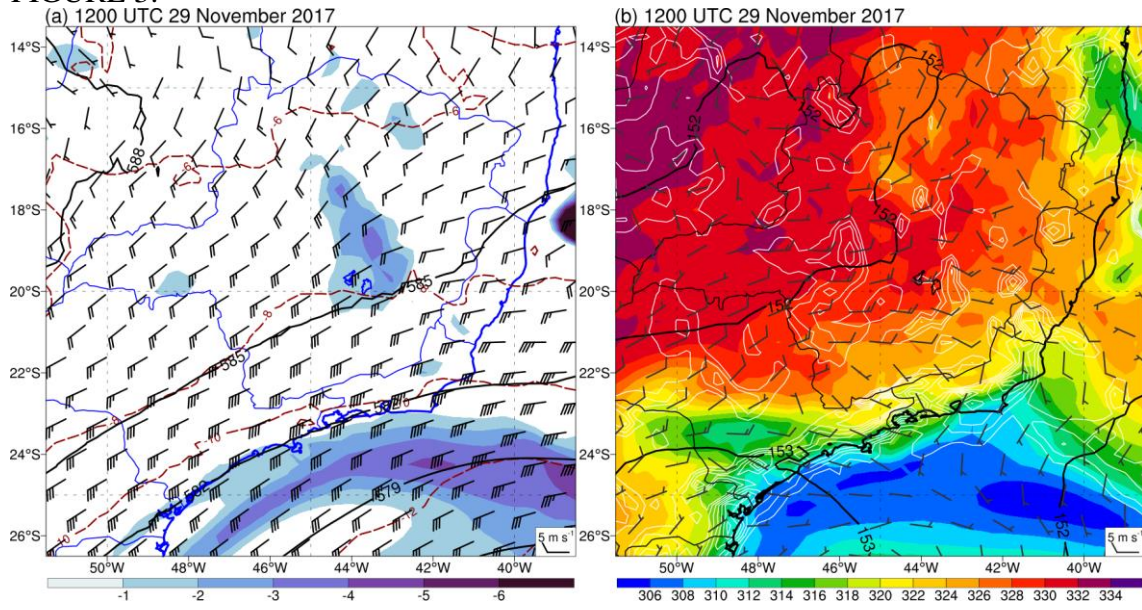


FIGURE 4:

SBCF 20171129 1200 UTC

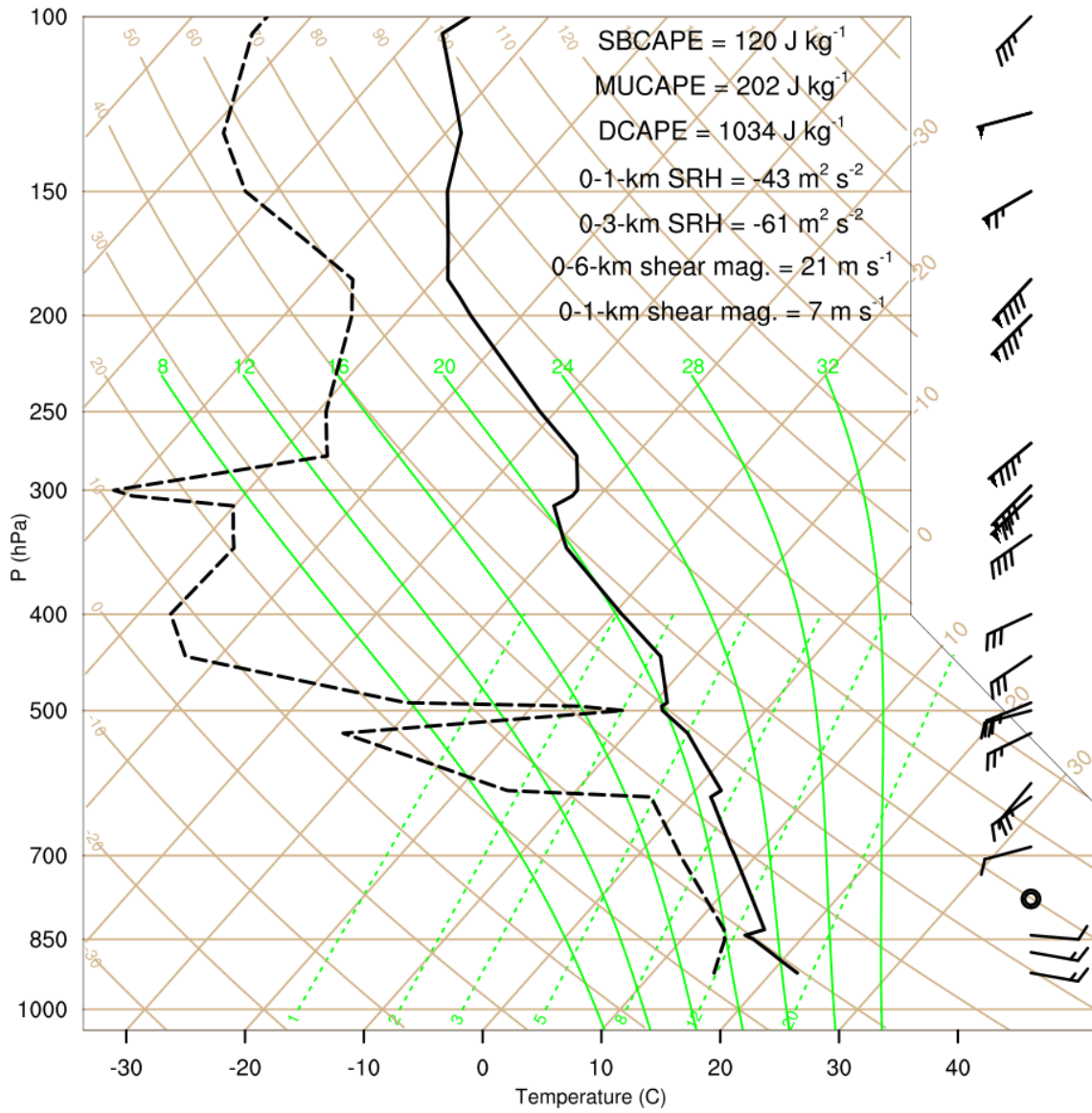


FIGURE 5:

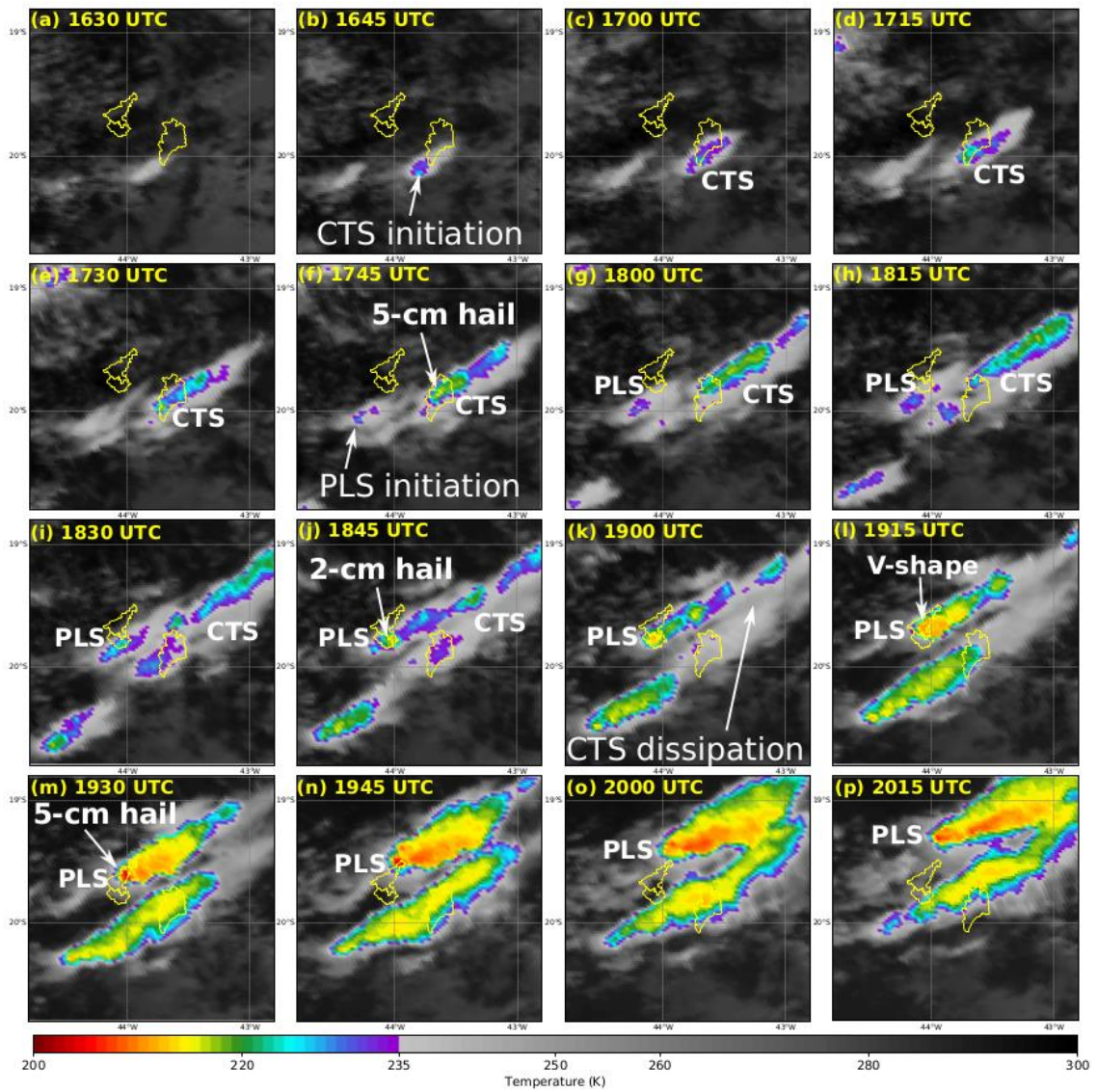


FIGURE 6:

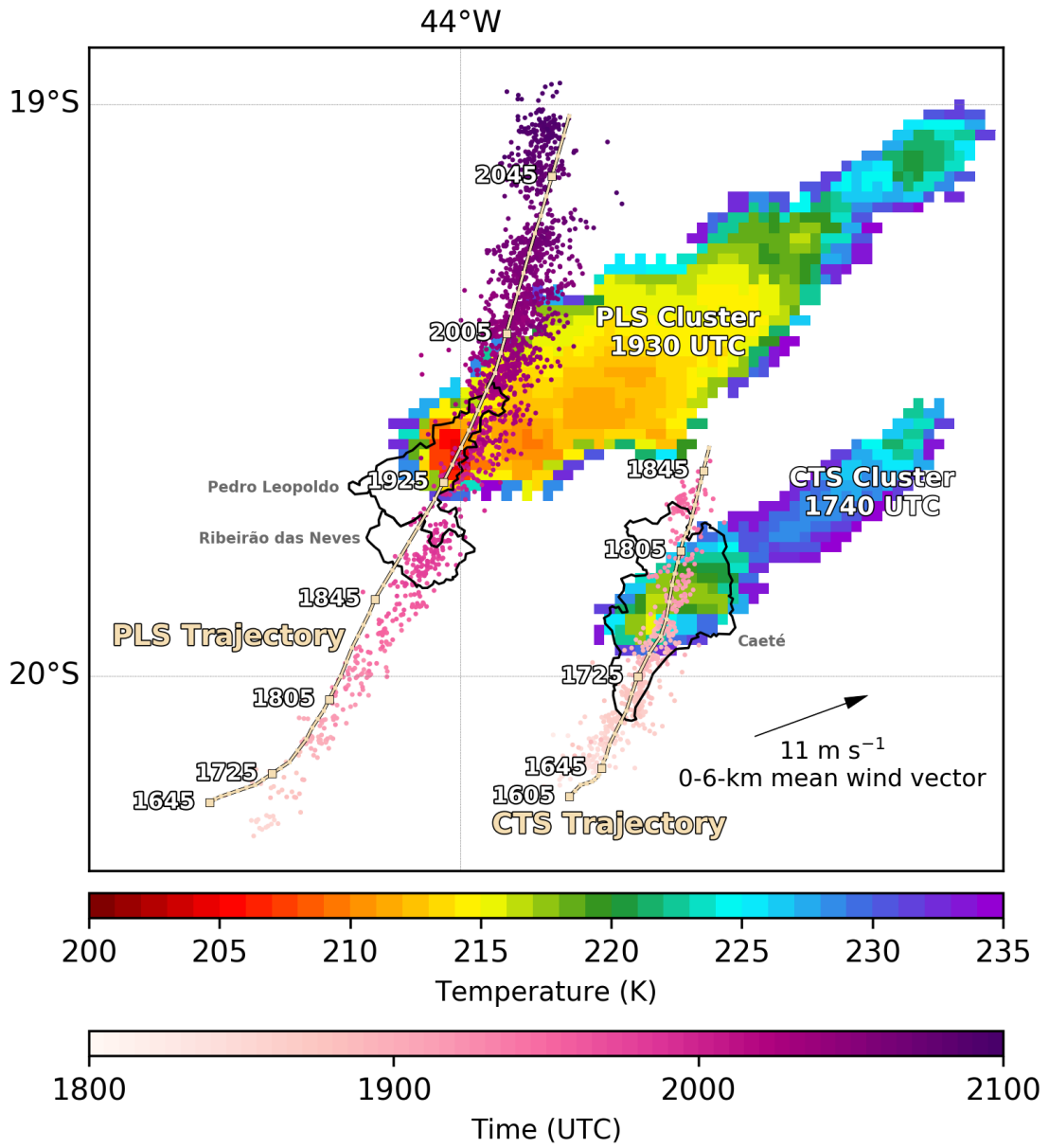


FIGURE 7:

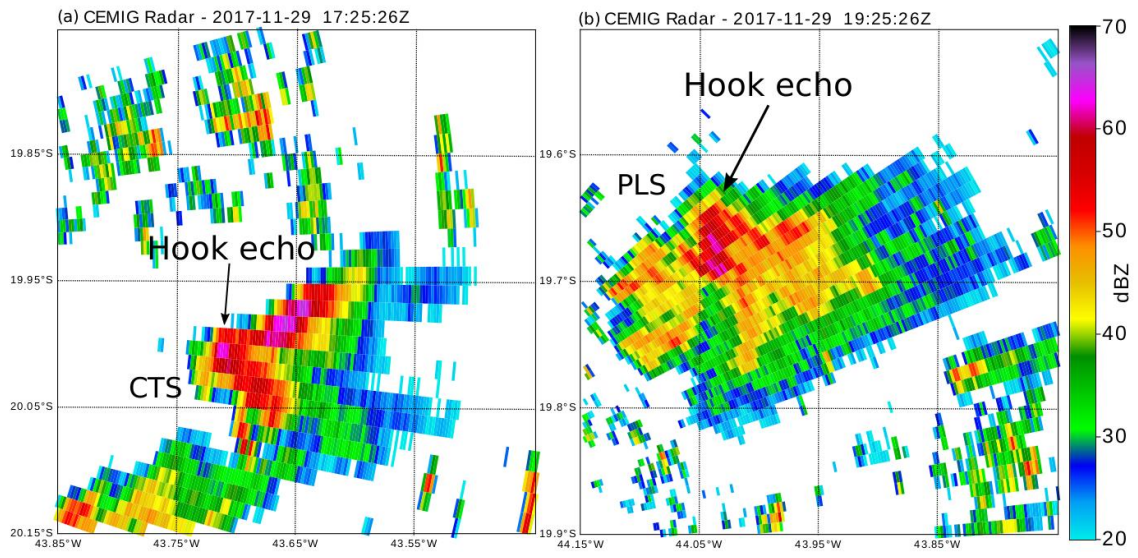


FIGURE 8:

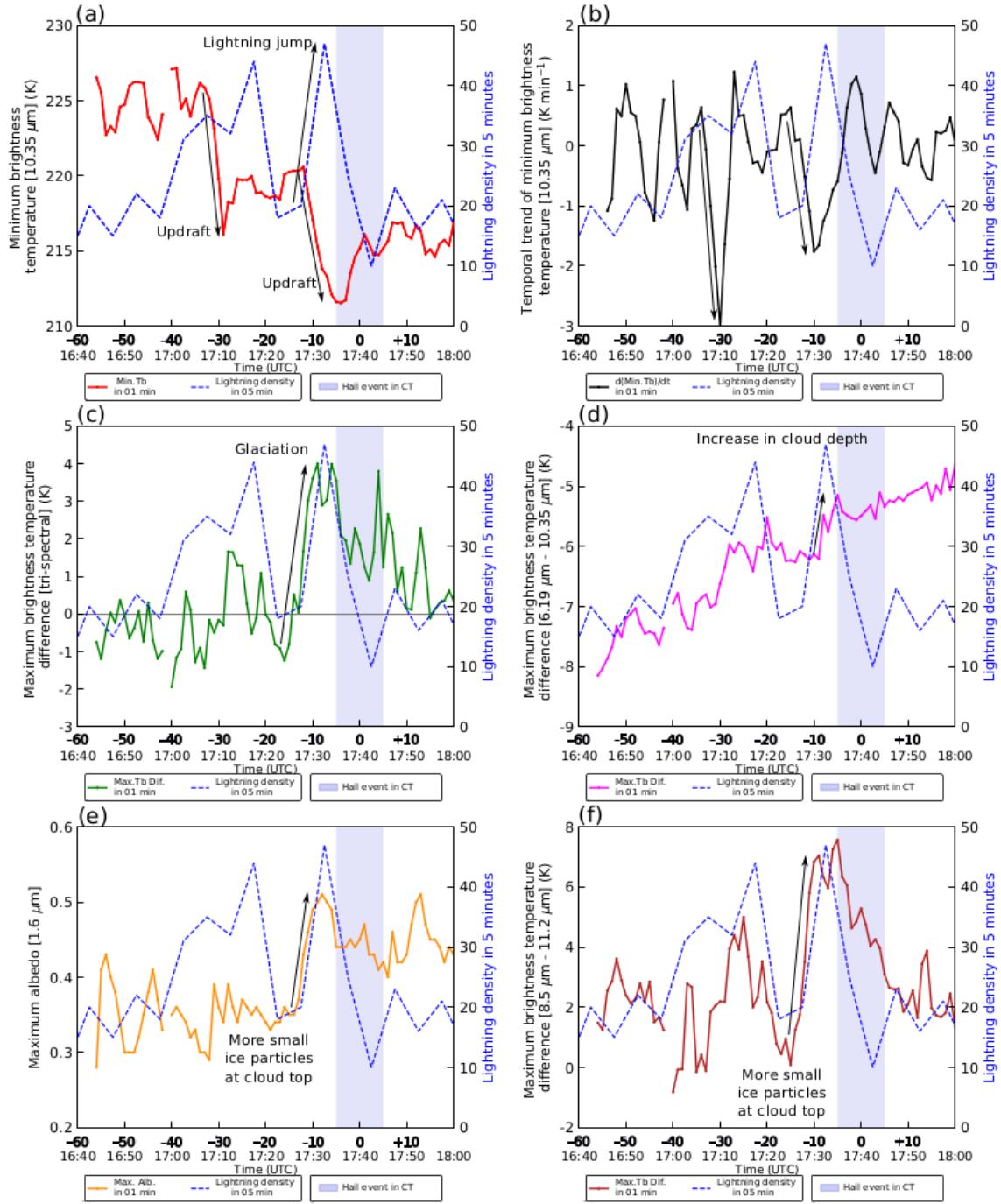


FIGURE 9:

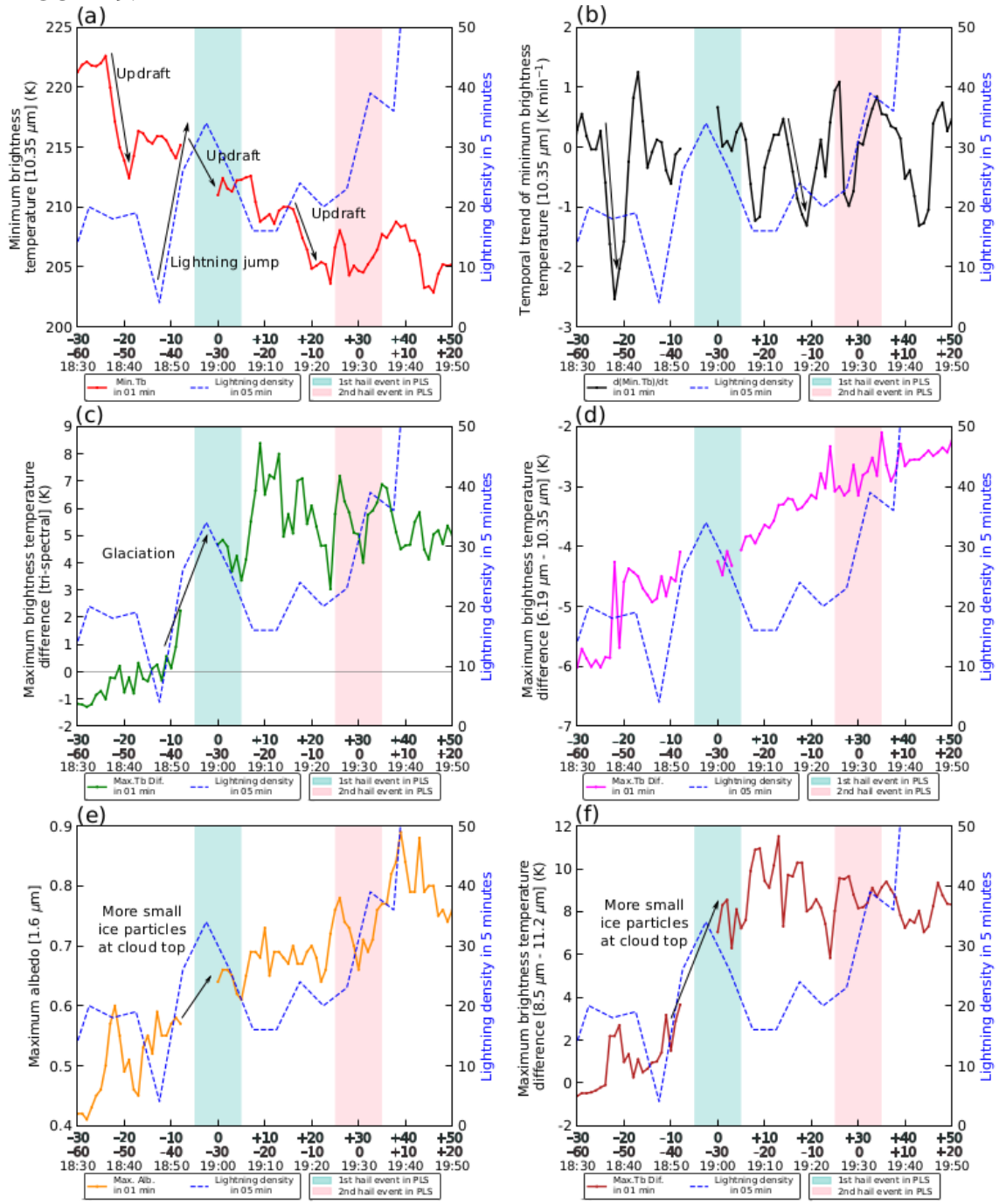


FIGURE 10:

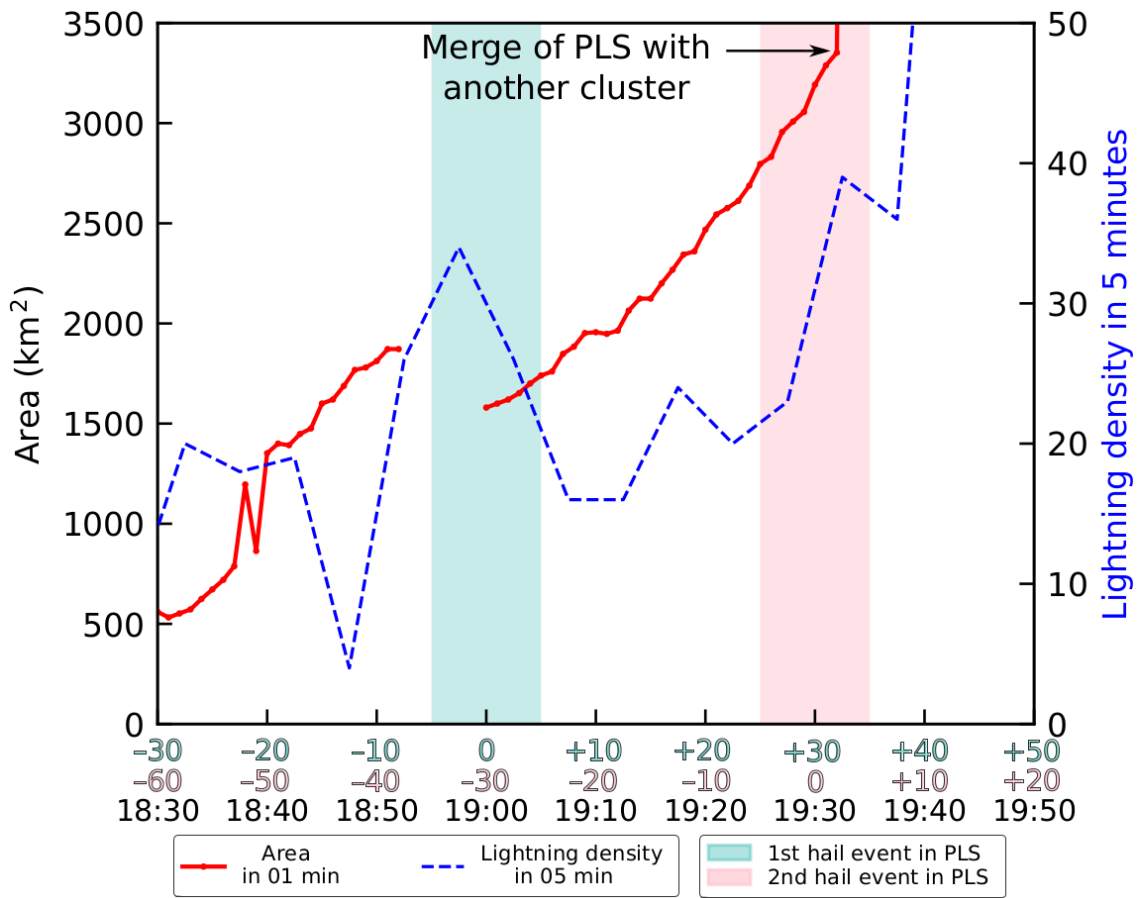


FIGURE 11:

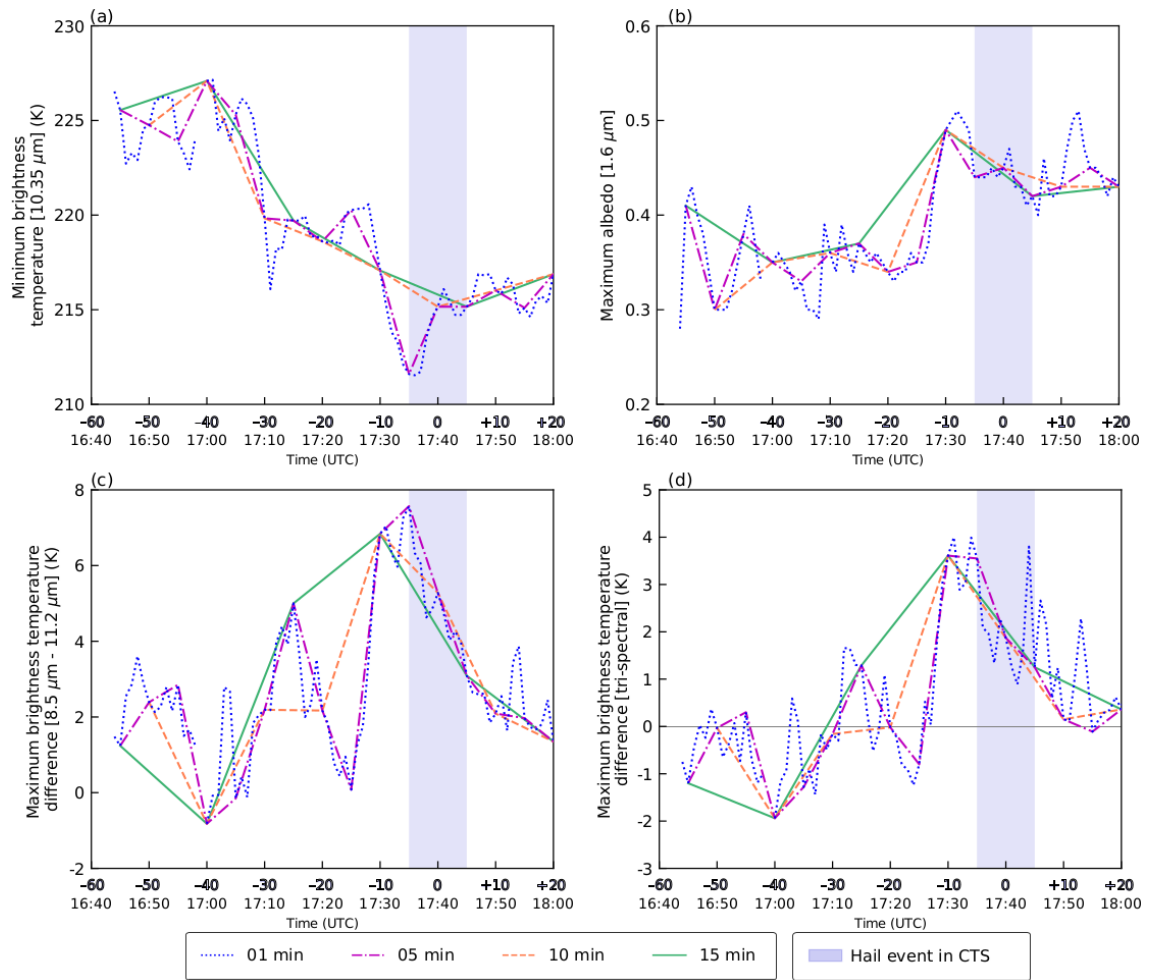


FIGURE 12:

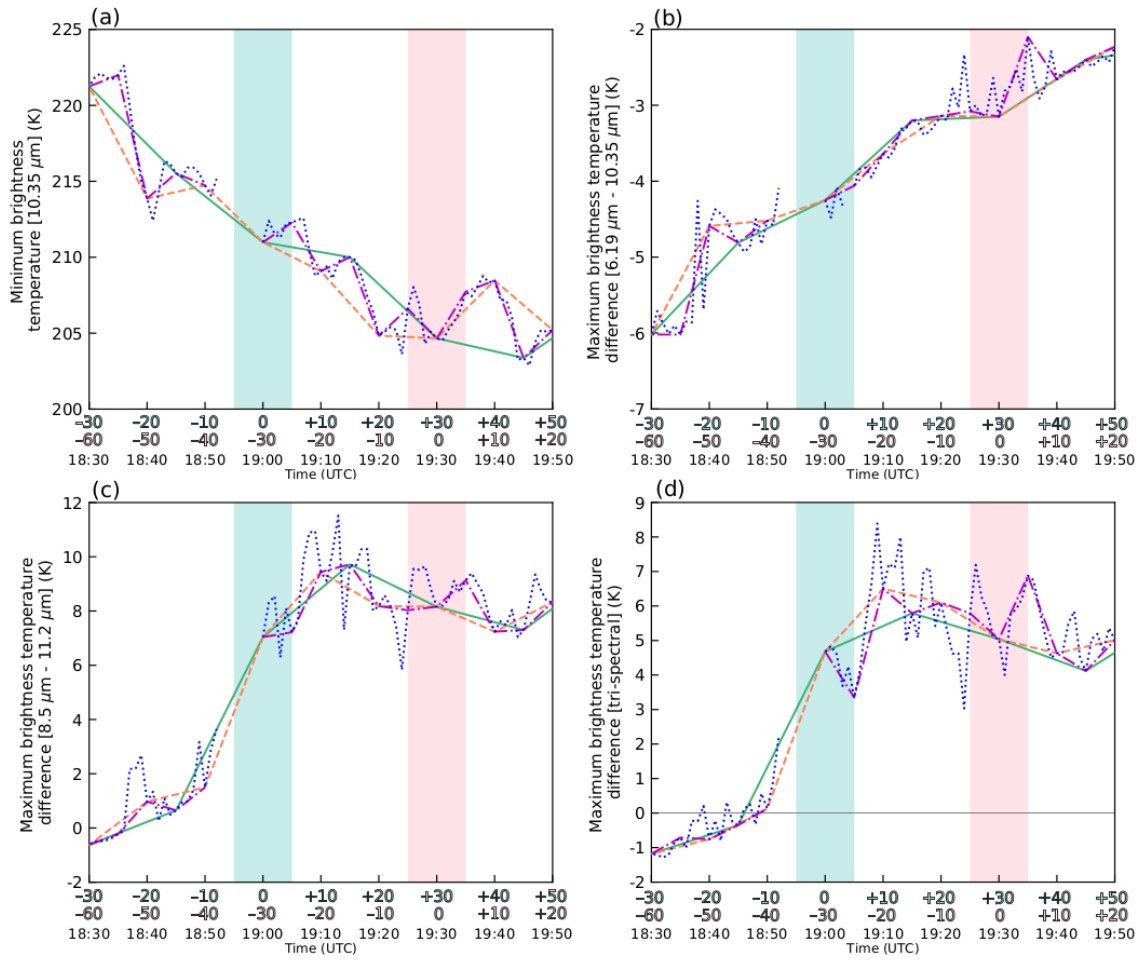


FIGURE 13:

